ELSEVIER

Chemical Engineering Journal 84 (2001) 485–490

Chemical Engineering Journal

www.elsevier.com/locate/cej

Experimental study on gas–liquid interfacial area and mass transfer coefficient in three-phase circulating fluidized beds

Weiguo Yang, Jinfu Wang*, Tiefeng Wang, Yong Jin

Department of Chemical Engineering, Tsinghua University, Beijing 100084, PR China

Received 15 November 1999; received in revised form 1 November 2000; accepted 6 November 2000

Abstract

The gas–liquid mass transfer behavior is studied in a three-phase circulating fluidized bed reactor of 140 mm i.d. and 3.0 m height. Using the oxygen dissolution method, the volumetric mass transfer coefficient $k_L a$ is obtained from the measured bulk concentration of the liquid phase by fitting to the axial dispersion model (ADM). The gas holdup and the distribution of bubble size in the bed are measured by a fiber optical probe system, then the gas–liquid interfacial area a and the mass transfer coefficient k_L are calculated. The influences of the main operating conditions, including superficial gas velocity, superficial liquid velocity and solid circulating rate, are studied systematically.

Keywords: Three-phase circulating fluidized bed; Gas–liquid mass transfer coefficient; Gas–liquid interfacial area

1. Introduction

Gas–liquid–solid three-phase fluidized beds have been widely used in chemical, petrochemical, electrochemical and biochemical processes. The most important operation mode of gas–liquid–solid fluidization is gas–liquid concurrent upward flow with liquid as continuous phase. In the past decades, investigations on this mode were mainly focused on conventional expanded bed regime [1]. However, the circulating/fast fluidization regime was less often studied.

For some gas–liquid–solid reaction systems, solid catalysts lose their activity due to the deposit of metal and coke on the surface. Hence, the particles should be carried out of the bed to be regenerated. Using an accompanying downcomer as a regenerator, the catalytic reaction and the regeneration of the catalysts can easily be coupled together by circulating operation and this two processes can be operated continuously. Liang et al. [2,3] presented the gas–liquid–solid three-phase fluidized bed with outer circulation of particles and studied its hydrodynamic behavior. Han et al. [4] and Yang et al. [5] studied the liquid phase flow structure and backmixing characteristics of gas–liquid–solid three-phase circulating fluidized bed.

Compared with the conventional fluidized bed, circulating fluidized bed reactors have many specific advantages, such as better interphase contact; reduced backmixing; higher gas/liquid velocity and larger processing capability; higher gas holdup; more uniform and more fine bubbles; more easily heat transfer into or out of the bed. These features exhibit that gas–liquid–solid three-phase circulating fluidized bed reactors have wide perspectives of potential application.

It is important for the development of three-phase circulating fluidized bed to acquire a good understanding of its gas–liquid mass transfer behavior. Up to now, a number of investigations on gas–liquid mass transfer of three-phase fluidization systems have been reported [6–12]. However, most research was limited to the measurement of gas–liquid volumetric mass transfer coefficient in the conventional expanded bed. For more clearly understanding the gas–liquid mass transfer behavior of three-phase circulating fluidized bed, it is essential to determine the gas–liquid volumetric mass transfer coefficient and the gas–liquid interfacial area simultaneously.

2. Experimental

2.1. Experimental apparatus

The experiments are carried out in a gas–liquid–solid three-phase fluidized bed shown in Fig. 1. The experimental apparatus consists of riser, liquid–solid separator, particle reservoir and liquid reservoir, etc. The riser is a vertical Plexiglas column of 140 mm i.d. and 3.0 m in height. Air, water and glass beads of 0.4 mm are used as the gas, liquid

* Corresponding author. Tel.: +86-10-62785464; fax: +86-10-62772051.
E-mail address: wangjfu@mail.tsinghua.edu.cn (J. Wang).

1385-8947/01/$ – see front matter
PII: S1385-8947(00)00374-0

Nomenclature

a	interfacial area (1 m)
c	dissolved oxygen concentration in the liquid phase (mg/l)
c^-	oxygen concentration at the bottom entrance (mg/l)
c^+	oxygen concentration above distributor at $x = 0$ (mg/l)
c^*	saturated oxygen concentration (mg/l)
d_p	particle diameter (mm)
D_Z	axial dispersion coefficient (cm^2/s)
F_{air}	mole flowrate of entrance air (mol/s)
G_s	particle-circulating rate (kg/m^2 s)
He	Henry constant (Pa l/mg)
k_L	gas–liquid mass transfer coefficient (m/s)
k_La	gas–liquid volumetric mass transfer coefficient (1 s)
L	column height (m)
P_0	atmospheric pressure (Pa)
Pe_L	Peclet number of liquid phase ($U_LL/D_Z\varepsilon_L$)
ΔP	pressure drop (Pa)
r	radial position (m)
R	radius of the bed (m)
Re_g	Reynold number of gas phase ($RU_g\rho_g/\mu_g$)
Re_L	Reynold number of liquid phase ($RU_L\rho_L/\mu_L$)
St_g	Stanton number of gas phase ($k_LaV_b/(32 \times 10^3F_{air})$
St_L	Stanton number of liquid phase (k_LaL/U_L)
U_g	superficial gas velocity (m/s)
U_L	superficial liquid velocity ($U_{L1} + U_{L2}$) (m/s)
U_{L1}	superficial primary liquid velocity (m/s)
U_{L2}	superficial secondary liquid velocity (m/s)
U_t	particle terminal velocity (m/s)
V_b	effective volume of column (46 l)
V_d	superficial solid velocity (G_s/ρ_s) (m/s)
x	axial coordinate (m)
x^*	dimensionless axial coordinate (x/L)
y	mole fraction of oxygen in gas phase

Greek letters

ε_g	gas holdup
ε_L	liquid holdup
ε_s	solid holdup
μ_g	gas viscosity
μ_L	liquid viscosity (kg/m^3)
ρ_g	gas density (kg/m^3)
ρ_L	liquid density (kg/m^3)
ρ_s	solid density (kg/m^3)

and solid phases, respectively. The liquid pumped from the reservoir is divided into two streams and then fed into the bed, a primary stream fed into the bed bottom and a secondary stream below the exit of the circulating standpipe, which is shown in Fig. 2. Solid particles entrained

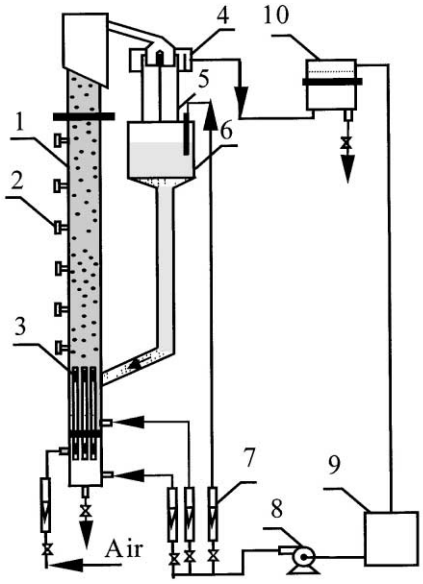

Fig. 1. Schematic diagram of the experimental apparatus: 1, riser; 2, pressure tap; 3, gas–liquid distributor; 4, liquid–solid separator; 5, particle metering tank; 6, particle reservoir; 7, flowmeter; 8, liquid pump; 9, liquid reservoir; 10, secondary liquid–solid separator.

from the top of the riser are separated from the liquid in a primary liquid–solid separator and returned to the reservoir. The particle-circulating rate is controlled by regulating the flow rate ratio between the two liquid streams.

2.2. Measurements

2.2.1. Measurement of the gas–liquid volumetric mass transfer coefficient

The gas–liquid volumetric mass transfer coefficient k_La is estimated by fitting the axial oxygen concentration distribution in the liquid phase according to the axial dispersion model (ADM), through simultaneous liquid

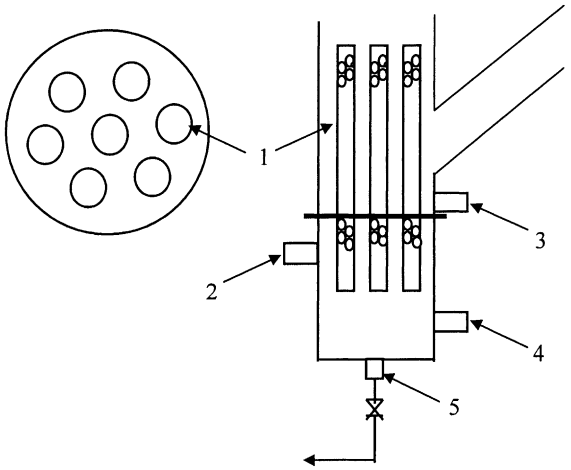

Fig. 2. Structure diagram of gas–liquid distributor: 1, gas–liquid distributing tube; 2, air inlet; 3, secondary liquid stream inlet; 4, primary liquid stream inlet; 5, drainage.

sampling at seven axial positions. The dissolved oxygen concentrations in the liquid phase are measured using a dissolved oxygen meter (JENWAY, model 9070). In order to determine the saturated solubility of oxygen in water, liquid temperatures are also measured. The oxygen in the fed water is stripped by pure nitrogen in the reservoir.

According to the ADM, the oxygen mass balance in the liquid phase of a three-phase fluidized bed can be written as [10]

$$\frac{1}{Pe_L}\frac{d^2c}{dx^{*2}} - \frac{dc}{dx^*} + St_L[(a - bx^*)y - c] = 0 \quad (1)$$

where $a = P_0/He$, $b = \Delta P/He$, $\Delta P = (\varepsilon_g\rho_g + \varepsilon_L\rho_L + \varepsilon_s\rho_s)_{gL}$.

The axial dispersion of oxygen in the gas phase can be neglected and the oxygen mass balance in the gas phase can be described by

$$\frac{dy}{dx^*} + St_g\left[\left(1 - \frac{b}{a}x^*\right)y - \frac{c}{a}\right] = 0 \quad (2)$$

where St_g is the Stanton number of the gas phase. The above mass balance Eqs. (1) and (2) are complemented with the following boundary conditions.

$$x^* = \begin{cases} 0, & c^+ = c^- + \dfrac{1}{Pe_L}\left.\dfrac{dc}{dx^*}\right|_{x^*=0}, \quad y = y_0 \\ 1, & \left.\dfrac{dc}{dx^*}\right|_{x^*=1} = 0 \end{cases} \quad (3)$$

The above two-point boundary value problem Eqs. (1)–(3) can be solved analytically or numerically. The axial distribution of c and y in the column can be calculated if c^-, Pe_L and k_La are given. In the present study, Pe_L is calculated according to the correlation by Han et al. [4].

$$Pe_L = 3.2 \times 10^{-4} Re_L Re_g^{-0.5}(1 - \varepsilon_s)^{2.8} \quad (4)$$

If the value of k_La is given appropriately, the axial distribution of dissolved oxygen concentration in the liquid phase will agree with experimental measurements. So the problem of determining k_La based on the measurement of dissolved oxygen concentration in the liquid phase, is converted to an optimization problem in which the target function is the error between the calculated and the measured oxygen concentrations.

$$\text{Err} = \sum_i (c_{i,\text{calc}} - c_{i,\text{meas}})^2 \rightarrow \min,$$
$$i = 0^+, 1, 2, \ldots, 7 \quad (5)$$

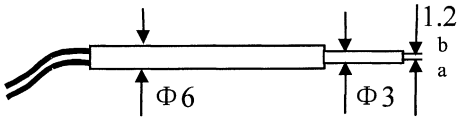

Fig. 3. Structure of the optical fiber probe: a, the upper fiber; b, the lower fiber.

2.2.2. Measurement of the gas–liquid interfacial area

The gas holdup ε_g and the bubble size distribution are measured by an optical fiber probe system for measuring the bubble behavior in multiphase flow. The mean bubble diameter d_b can be deduced from the bubble size distribution and the gas–liquid interfacial area a can be calculated by the expression of $a = 6\varepsilon_g/d_b$. Then, the gas–liquid mass transfer coefficient k_L can be obtained.

The optical fiber probe system mainly consists of laser source, light splitter, optical fiber coupler, light detector, amplifier, A/D transducer, optical fiber probe and PC. A single beam of laser emitted by the continuous infrared laser source is separated into two beams by the light splitter. These two beams of laser enter the optical fiber through the coupler and are reflected on the top of probe. The intensities of the reflection light are different when the probe is placed in gas phase and liquid phase. The light detector converts the signals of light intensity into the electrical signals. Then the standard 0–5 V voltage signals are obtained after amplification and offset treatment. These original signals can be sampled by a PC after the A/D conversion.

The structure of the probe is shown in Fig. 3. It is made up of a pair of communication optical fiber of 62.5 μm in diameter. It can move in the radial direction and measure the radial distribution of bubble size from the center to the wall of the column. Before it was used for three-phase measurement, the probe was calibrated in a two-dimensional gas–liquid bubble column. Fig. 4 shows a set of typical signals from the probe measured in the three-phase fluidized bed.

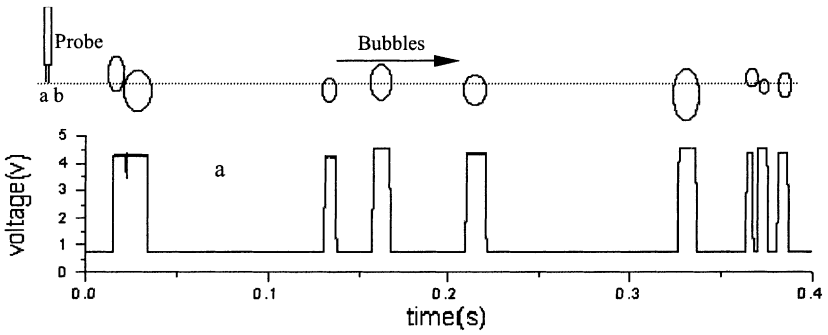

Fig. 4. Typical signals from the optical fiber probe.

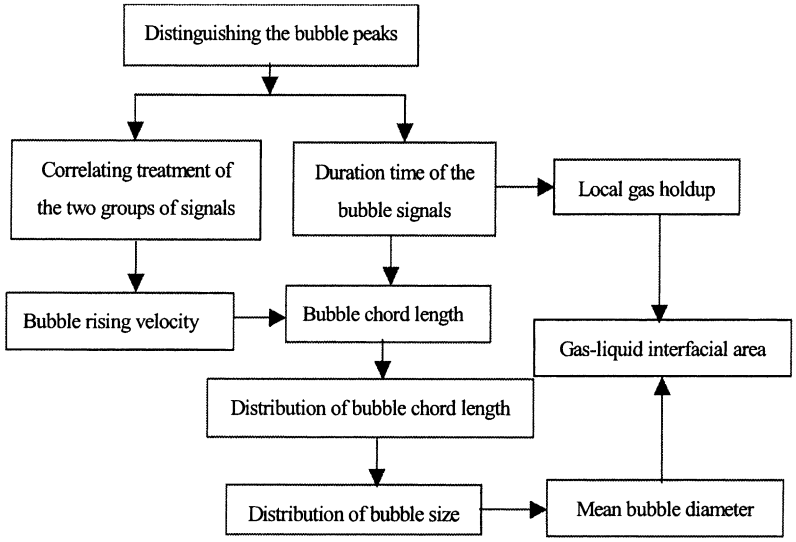

Fig. 5. Program frame of data treatment process.

As shown in Fig. 5, the bubble peaks are first distinguished from the original data. Then the local gas holdup, the bubble rising velocity, the distribution of bubble chord length and the distribution of bubble size can be obtained after the arithmetic treatment of correlation, statistics and distributing transformation. The local gas holdup is determined by integrating the measured values over 0 to R. The distribution of bubble chord length is transformed to the distribution of bubble size by using the method of Liu et al. [13]. Based on the local gas holdup and the distribution of bubble size, the gas–liquid interfacial area can be calculated.

3. Results and discussion

3.1. Influence of superficial gas velocity

It can be seen in Figs. 6 and 7 that the superficial gas velocity has remarkable influence on gas–liquid mass transfer behavior in the three-phase circulating fluidized bed. Both the gas–liquid interfacial area and the gas–liquid mass transfer coefficient increase with increasing superficial gas velocity. The reason is that higher gas velocity increases the gas holdup and decreases the mean diameter of bubble, leading to the increase of gas–liquid interfacial area. In addition, the increase of gas velocity speeds up the rising velocity of bubbles in the bed and enhances the turbulence of the liquid phase around the rising bubbles. The mass transfer resistance from the liquid film on the surface of bubbles to the liquid bulk decreases, then the gas–liquid mass transfer coefficient increases.

3.2. Influence of superficial liquid velocity

Figs. 8 and 9 illustrate the influence of superficial liquid velocity on the gas–liquid interfacial area and the gas–liquid mass transfer coefficient. The superficial liquid velocity

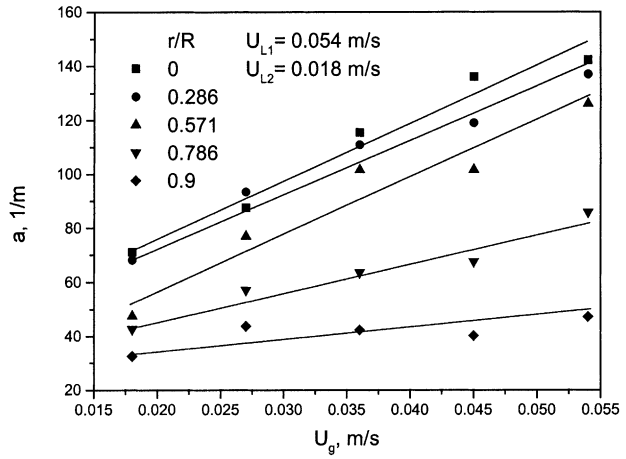

Fig. 6. The effect of superficial gas velocity on the gas–liquid interfacial area at different radial positions.

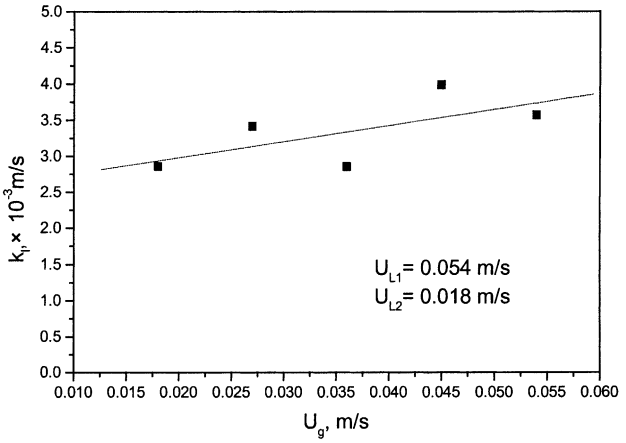

Fig. 7. The variation of gas–liquid mass transfer coefficient with superficial gas velocity.

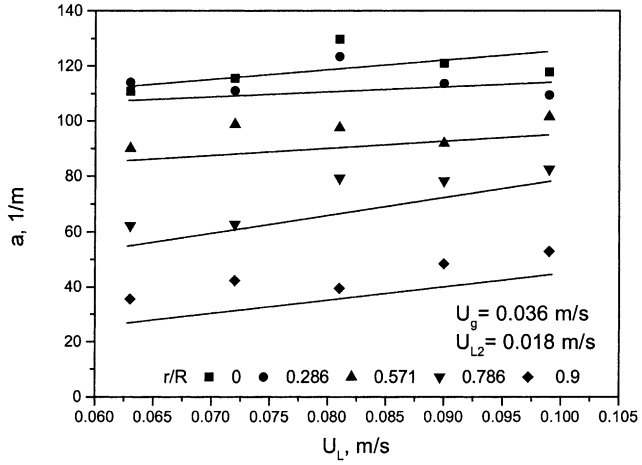

Fig. 8. The effect of superficial liquid velocity on the gas–liquid interfacial area at different radial positions.

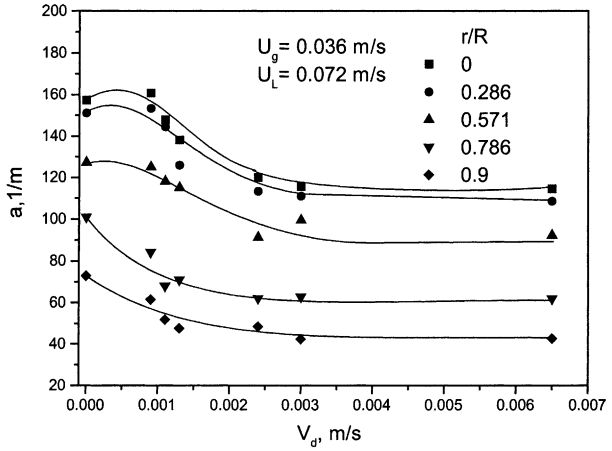

Fig. 10. The effect of particle circulating rate on the gas–liquid interfacial area at different radial positions.

has a little influence on the gas–liquid interfacial area. The gas–liquid interfacial area of the wall region increases slightly with the increase of liquid velocity, but that of the center region changes little. As a result of small influence of liquid velocity on the mean bubble diameter, the variation of the gas–liquid interfacial area is determined by the influence of liquid velocity on the gas holdup. Increasing liquid velocity enhances the gas holdup of the wall region, so the gas–liquid interfacial area of the wall region increases. A nearly linear variation of gas–liquid mass transfer coefficient versus superficial liquid velocity is found within a certain range of the superficial liquid velocity, similar to the variation of gas–liquid mass transfer coefficient versus superficial gas velocity. The reason is that higher liquid velocity promotes the turbulence degree of liquid flow just like the increase of gas velocity. Then the mass transfer liquid film in the system becomes thinner and the gas–liquid mass transfer of the liquid side increases.

3.3. Influence of solid holdup

In the three-phase circulating fluidized bed, the solid holdup can be regulated through controlling the flowrate ratio of the main liquid flow and the secondary liquid flow to alter the particle circulating rate. According to the work of Liang et al. [3], the solid holdup can be increased by increasing the particle circulating rate, that is increasing the secondary liquid velocity.

It can be seen in Fig. 10 that increasing particle circulating rate results in the increase of solid holdup and the decrease of gas–liquid interfacial area. The reason is that the increase of solid holdup leads to increasing the system apparent viscosity and the bubble coalescence will be increased consequently. However, the influence of solid holdup on the gas–liquid mass transfer coefficient is relatively complex. As shown in Fig. 11, the gas–liquid mass

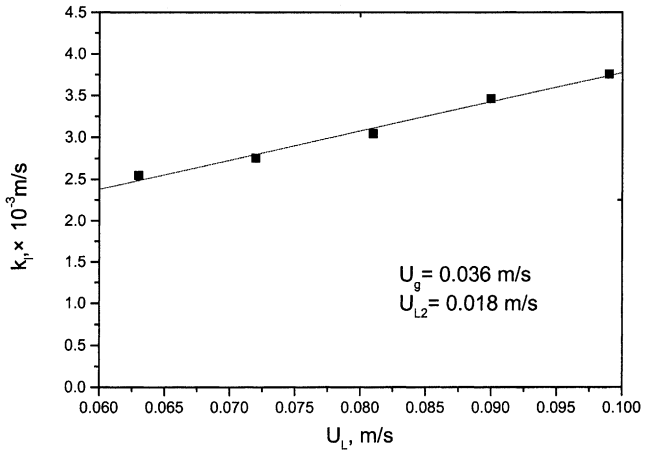

Fig. 9. The variation of gas–liquid mass transfer coefficient with superficial liquid velocity.

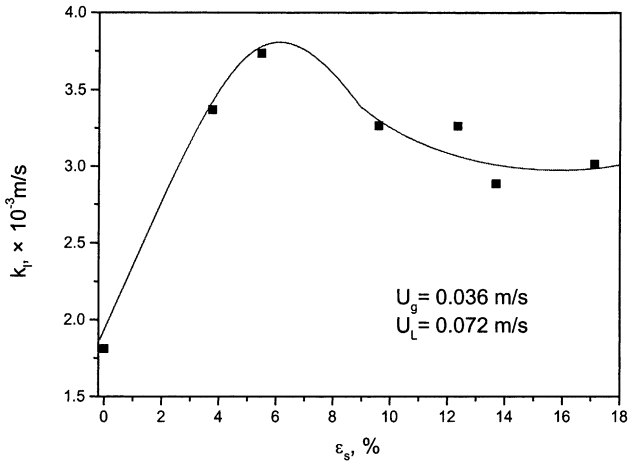

Fig. 11. The variation of gas–liquid mass transfer coefficient with solid holdup.

transfer coefficient increases greatly with the increase of solid holdup when the solid holdup is small; but it decreases slowly with the further increase of solid holdup. In the region of low solid holdup, the existence and movement of particles takes the effect of breaking bubbles and enhancing the turbulence of liquid phase, then the capacity of gas–liquid mass transfer increases. In the region of high solid holdup, the enhancement of solid holdup results in increasing the apparent viscosity of the bed, which is unfavorable to the mass transfer process, since gas–liquid mass transfer coefficient is inversely proportional to viscosity [14], then the gas–liquid mass transfer coefficient decreases.

4. Conclusions

Using the oxygen dissolution method and a fiber optical probe system, the gas–liquid volumetric mass transfer coefficient and the gas–liquid interfacial area can be measured simultaneously in the three-phase circulating fluidized bed. Study on the effect of main operation conditions on the gas–liquid mass transfer coefficient comes into the following conclusions.

1. The gas–liquid mass transfer coefficient increases with increasing superficial gas velocity.
2. The gas–liquid mass transfer coefficient increases with increasing superficial liquid velocity.
3. There is a maximal value of gas–liquid mass transfer coefficient as the particle circulating rate increases: in the region of low solid holdup, the gas–liquid mass transfer coefficient increases with increasing solid holdup, in the region of high solid holdup, the gas–liquid mass transfer coefficient decreases with increasing solid holdup.

Acknowledgements

This study was supported by the Chinese National Natural Science Foundation No. 29876019.

References

[1] L.S. Fan, Gas–Liquid–Solid Fluidization Engineering, Butterworths, London, MA, USA, 1989.
[2] W.G. Liang, Q.W. Wu, Z.Q. Yu, Y. Jin, H.T. Bi, AIChE J. 41 (1995) 267.
[3] W.G. Liang, Q.W. Wu, Z.Q. Yu, Y. Jin, Z.W. Wang, Can. J. Chem. Eng. 73 (1995) 656.
[4] S.J. Han, J. Zhou, W.G. Yang, Y. Jin, Z.W. Wang, J. Chem. Ind. Eng. (China) 48 (1997) 477.
[5] W.G. Yang, J.F. Wang, W. Chen, Y. Jin, Chem. Eng. Sci. 54 (1999) 5293.
[6] K. Østergaard, W. Suchozebrsk, in: Proceedings of the 4th European Symposium on Chemical Reaction Engineering, Pergamon Press, Oxford, 1971, p. 21.
[7] V.R. Dhanuka, J.B. Stepanek, AIChE J. 26 (1980) 1029.
[8] K. Nguyen-Tien, A.N. Patwari, A. Schumpe, W.D. Deckwer, AIChE J. 31 (1985) 194.
[9] S.K. Chang, Y. Kang, S.D. Kim, J. Chem. Eng. Jpn. 19 (1986) 524.
[10] J.O. Kim, S.D. Kim, Can. J. Chem. Eng. 68 (1990) 368.
[11] D.H. Lee, J. Kim, S.D. Kim, Chem. Eng. Commun. 119 (1993) 179.
[12] W.G. Yang, J.F. Wang, L.M. Zhou, Y. Jin, Chem. Eng. Sci. 54 (1999) 5523.
[13] W.D. Liu, N.N. Clark, A.I. Karamavruc, Chem. Eng. Sci. 53 (1998) 1267.
[14] P.H. Calderbank, M.B. Moo-Young, Chem. Eng. Sci. 39 (1961) 39.